ELSEVIER

11 February 2002

Physics Letters A 294 (2002) 19–25

PHYSICS LETTERS A

www.elsevier.com/locate/pla

Effect of concentration of the Er^{3+} ion on electromagnetically induced transparency in Er^{3+}:YAG crystal

Huailiang Xu *, Zhenwen Dai, Zhankui Jiang

Department of Physics, Jilin University, Jiefang Road 119, Chang Chun 130023, PR China

Received 3 August 2001; received in revised form 6 November 2001; accepted 5 December 2001

Communicated by P.R. Holland

Abstract

We studied the effect of Er^{3+} concentration on electromagnetically induced transparency in two types of three-level schemes—the ladder and the Λ models in Er^{3+}:YAG. The numerical calculations show that, under the same intensities of the probe and the coupling fields, the absorption and the dispersion were dramatically changed with Er^{3+} concentration. © 2002 Elsevier Science B.V. All rights reserved.

PACS: 42.50.Hz; 42.50.Gy; 42.70.Mp

Keywords: EIT; Er^{3+}:YAG; Concentration

1. Introduction

Quantum coherence has led to many interesting optical phenomena such as electromagnetically induced transparency (EIT) [1–4], lasing without population inversion [5,6], and the enhancement of refractive index [7,8]. The effect termed EIT is an induced transparency in an initially absorbing medium, experienced by a weak-probe field, due to the presence of a strong-coupling field on a linked transition. Most experimental studies on EIT have focused on atomic gas media. Recently, the experimental observations of EIT and pertained phenomena in solid have also appeared [9–15]. However, all of these experiments in solid crystals were carried out under the same concentration of doped ions. Here we may now propose such a question: What is the effect of the concentration of doped ions on EIT? The purpose of this Letter is to examine the above question regarding EIT in Er^{3+}:YAG and to provide a basis for choosing the appropriate concentration of Er^{3+} doped ions. YAG is a good host material and superior in terms of hardness and thermal conductivity. It has a cubic space-group symmetry of O_h^{10} and the Er^{3+} ions substitute for Y^{3+} ions on the dodecahedral sites having D_2 symmetry [16].

In the rare-earth doped crystal, the decay rate of population and electric dipole moment vary as a function of the concentration due to the influence of some factors, such as phonon decay and the interaction among ions [17]. In this Letter we conduct a systematic study of the effect of concentration of Er^{3+} ions on the EIT on the basis of the density matrix theory, in which the dopant concentration is a variable parameter. We focus our attention on two types of ideal

* Corresponding author.
E-mail address: jzk@mail.jlu.edu.cn (Z. Jiang).

0375-9601/02/$ – see front matter
PII: S0375-9601(01)00828-3

closed three-level schemes, the ladder and Λ models, in which the absorption and dispersion properties of Er^{3+}:YAG were obtained by the numerical solution of their density matrix equations.

2. Theory

In this section we discuss the theoretical basis for our calculations dealing with the effect of concentration on EIT in two closed three-level schemes, the ladder and the Λ models, as shown in Fig. 1. The energy-level schemes are relevant to the Er^{3+} ions in Er^{3+}:YAG, where the levels $|1\rangle$, $|2\rangle$ and $|3\rangle$ correspond to the lowest Stark level of the $^4I_{15/2}$, $^4I_{13/2}$ and $^4S_{3/2}$ states, respectively. A strong coherent coupling field E_c with Rabi frequency G_c couples levels $|2\rangle$ and $|3\rangle$. A weak probe field E_p with Rabi frequency G_p induces the transition $|1\rangle \leftrightarrow |2\rangle$ for the ladder model and $|1\rangle \leftrightarrow |3\rangle$ for the Λ model. The interaction between atom and field was, in general, treated in the interacting picture. In the following, we consider the ladder model and the Λ model, separately.

2.1. Ladder model

The interaction Hamiltonian for this model in the rotating-wave approximation can be written as

$$H_{\text{ladd}} = \hbar\Delta_p|2\rangle\langle 2| + \hbar(\Delta_p + \Delta_c)|3\rangle\langle 3| - \hbar\big(G_p|2\rangle\langle 1| + G_c|3\rangle\langle 2| + \text{c.c.}\big), \quad (1)$$

where Δ_p and Δ_c are the frequency detuning of the probe and coupling fields, respectively, and $\Delta_p = \omega_{21} - \omega_p$, $\Delta_c = \omega_{32} - \omega_c$ (ω_{ij} is the transition frequency between level $|i\rangle$ and $|j\rangle$; ω_p, ω_c are the frequencies of the probe and coupling fields, respectively). The time-dependence density matrix equation of motion is

$$\frac{d\rho}{dt} = -\frac{i}{\hbar}[H_I, \rho] - \frac{1}{2}\{\Gamma, \rho\}, \quad (2)$$

where $\{\Gamma, \rho\} = \Gamma\rho + \rho\Gamma$ [15]. The resulting equations for the density-matrix elements can be given by

$$\dot\rho_{11} = (\Gamma_{21} + \gamma_2)\rho_{22} + \Gamma_{31}\rho_{33} + iG_p^*\rho_{21} - iG_p\rho_{12},$$
$$\dot\rho_{22} = -(\Gamma_{21} + \gamma_2)\rho_{22} + (\Gamma_{32} + \gamma_3)\rho_{33} - iG_p^*\rho_{21} + iG_p\rho_{12} + iG_c^*\rho_{32} - iG_c\rho_{23},$$

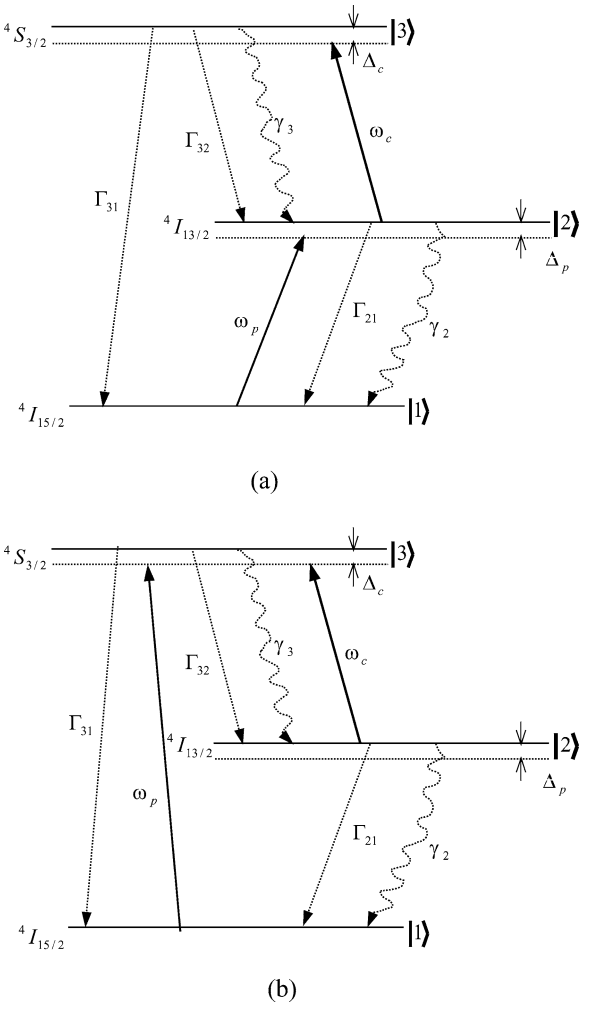

Fig. 1. Partial energy-level diagram of Er^{3+} in Er^{3+}:YAG showing the schemes employed for (a) the ladder and (b) the Λ models. γ_2, γ_3 are nonradiative decay rates of $|2\rangle$ and $|3\rangle$ levels, respectively. Γ_{ij} is the spontaneous transition probability from level i to level j. Δ_p, Δ_c are the detuning of the probe and the coupling fields.

$$\dot\rho_{21} = -(\gamma_{21} + i\Delta_p)\rho_{21} + iG_p(\rho_{11} - \rho_{22}) + iG_c^*\rho_{31},$$
$$\dot\rho_{31} = -\big[\gamma_{31} + i(\Delta_p + \Delta_c)\big]\rho_{31} - iG_p\rho_{32} + iG_c\rho_{21},$$
$$\dot\rho_{32} = -(\gamma_{32} + i\Delta_c)\rho_{32} + iG_c(\rho_{22} - \rho_{33}) - iG_p^*\rho_{31},$$
$$\rho_{ij} = \rho_{ji}^*,$$
$$\rho_{11} + \rho_{22} + \rho_{33} = 1, \quad (3)$$

where γ_i are nonradiative decay rate of level i, Γ_{ij} is the spontaneous transition probability from level i to level j. The coherence decay rates (γ_{ij}) are obtained according to the relations $\gamma_{21} = (1/2)(\Gamma_{21} + \gamma_2)$,

$\gamma_{31} = (1/2)(\Gamma_{31} + \Gamma_{32} + \gamma_3)$ and $\gamma_{32} = (1/2)(\Gamma_{31} + \Gamma_{32} + \Gamma_{21} + \gamma_2 + \gamma_3)$. The Rabi frequencies are defined by

$$G_p = \frac{\mu_{12} E_p}{2\hbar}, \tag{4a}$$

$$G_c = \frac{\mu_{23} E_c}{2\hbar}, \tag{4b}$$

where μ_{ij} is the electric dipole element between level i and level j of Er^{3+} ion, which can be given by [18, 19]

$$\begin{aligned}\mu_{ij}^2 &= e^2 \left|\langle \psi | r | \psi' \rangle\right|^2 \\ &= \frac{2}{(2J+1)} \frac{2}{(2J'+1)} e^2 \\ &\quad \times \sum_{\lambda=2,4,6} \Omega_\lambda \left|\left\langle 4f^N(\alpha SL) J \right\| U^\lambda \right. \\ &\qquad \left. \times \left\| 4f^N(\alpha' S' L') J' \right\rangle\right|^2, \end{aligned} \tag{5}$$

where Ω_λ is the phenomenological intensity parameter, J is the quantum number of angular momentum of the state j. The factors 2 in Eq. (5) arose from the Kramers degenerate of the Stark levels of Er^{3+}. The reduced matrix element U^λ can be obtained from Ref. [20] and the spectral intensity parameters can be described by an empirical formula [21]

$$\Omega_\lambda\left(10^{-20}\right) = 1.25 X^{1/4} \exp\left[-0.4(X-A)^{2/3}\right] + B, \tag{6}$$

where X is the concentration of doped ions. A and B are empirical parameters: $A = 1.0$, $B = 0.33$ for Ω_2, $A = 1.1$, $B = 0.72$ for Ω_4, and $A = 1.4$, $B = 0.59$ for Ω_6. The absorption and dispersion of the probe field can be described as [22]

$$\chi'' = \mathrm{Im}\left(\frac{2N\mu_{12}\rho_{21}}{\varepsilon_0 E_p}\right), \tag{7a}$$

$$\chi' = \mathrm{Re}\left(\frac{2N\mu_{12}\rho_{21}}{\varepsilon_0 E_p}\right), \tag{7b}$$

where N is the number of doped ions per unit volume and is proportional to the concentration of Er^{3+} ion.

2.2. Λ model

The Hamiltonian for this model in the rotating frame can be described as

$$\begin{aligned} H_\Lambda &= \hbar(\Delta_p - \Delta_c)|2\rangle\langle 2| + \hbar\Delta_p|3\rangle\langle 3| \\ &\quad - \hbar\left(G_p|3\rangle\langle 1| + G_c|3\rangle\langle 2| + \text{c.c.}\right), \end{aligned} \tag{8}$$

where $\Delta_p = \omega_{31} - \omega_p$, $\Delta_c = \omega_{32} - \omega_c$. The resulting density matrix equations are given by

$$\begin{aligned} \dot\rho_{11} &= (\Gamma_{21} + \gamma_2)\rho_{22} + \Gamma_{31}\rho_{33} + iG_p^*\rho_{31} - iG_p\rho_{13}, \\ \dot\rho_{22} &= -(\Gamma_{21} + \gamma_2)\rho_{22} + (\Gamma_{32} + \gamma_3)\rho_{33} + iG_c^*\rho_{32} \\ &\quad - iG_c\rho_{23}, \\ \dot\rho_{21} &= -\left[\gamma_{21} + i(\Delta_p - \Delta_c)\right]\rho_{21} - iG_p\rho_{23} + iG_c^*\rho_{31}, \\ \dot\rho_{31} &= -(\gamma_{31} + i\Delta_p)\rho_{31} + iG_p(\rho_{11} - \rho_{33}) + iG_c\rho_{21}, \\ \dot\rho_{32} &= -(\gamma_{32} + i\Delta_c)\rho_{32} + iG_c(\rho_{22} - \rho_{33}) + iG_p\rho_{12}, \\ \rho_{ij} &= \rho_{ji}^*, \\ \rho_{11} + \rho_{22} + \rho_{33} &= 1, \end{aligned} \tag{9}$$

where the meanings of the parameters γ_i, Γ_{ij} and γ_{ij} are the same as Eqs. (3). The Rabi frequencies are defined as

$$G_p = \frac{\mu_{13} E_p}{2\hbar}, \tag{10a}$$

$$G_c = \frac{\mu_{23} E_c}{2\hbar}. \tag{10b}$$

The absorption and dispersion of the probe field for this system can be described as

$$\chi'' = \mathrm{Im}\left(\frac{2N\mu_{13}\rho_{31}}{\varepsilon_0 E_p}\right), \tag{11a}$$

$$\chi' = \mathrm{Re}\left(\frac{2N\mu_{13}\rho_{31}}{\varepsilon_0 E_p}\right). \tag{11b}$$

3. Results and discussion

The spectral intensity parameters and the electric dipole moments under different concentrations have been calculated using Eqs. (5) and (6), and are listed in Table 1. From Refs. [17,21], we found that $\Gamma_{31} \ll \gamma_3$ due to the multi-phonon decay in this crystal. Therefore, it is reasonable for the crystal used to set the parameters as $\Gamma_{31} = 0$, $\Gamma_{31} + \gamma_2 = 1/\tau_2$ and $\Gamma_{32} + \gamma_3 = 1/\tau_3$, where the experimental lifetime values (τ_2, τ_3) of levels 2 and 3 under different concentrations have been obtained from Ref. [17] and also listed in Table 1. The Rabi frequency can be obtained from Eqs. (4) and (10), where the intensities of the probe and the coupling fields were being kept constant for all concentration of doped ions and setting

$$\frac{E_p}{2\hbar} = \frac{1}{10}\frac{1}{\mu_{12}}\frac{1}{\tau_2}$$

Table 1
Spectral intensity parameters, electrical dipole moments and population decay rates in Er^{3+}:YAG crystals containing different concentrations of the Er^{3+} ion

Concentration of Er^{3+} ion in crystal (at%)	Spectral intensity parameters (10^{-20} cm^2)			Electric dipole moments (10^{-32} C m)			Lifetime (μs) [17]	
	Ω_2	Ω_4	Ω_6	μ_{12}	μ_{13}	μ_{23}	$^4I_{13/2}$	$^4S_{3/2}$
0.5	1.15	1.51	1.31	3.25	1.59	1.69	6.5	14
3	1.20	1.61	1.54	3.81	1.72	1.84	9.0	10.5
15	0.57	0.96	0.84	2.82	1.27	1.36	9.0	1
33	0.38	0.77	0.64	2.47	1.11	1.19	2.0	0.5
100	0.33	0.72	0.59	2.36	1.06	1.14	0.28	0.05

for the ladder model,

$$\frac{E_p}{2\hbar} = \frac{1}{10}\frac{1}{\mu_{13}}\frac{1}{\tau_2}$$

for the Λ model and

$$\frac{E_c}{2\hbar} = 20\frac{1}{\mu_{23}}\frac{1}{\tau_2}$$

for both of these models (τ_2 and μ_{ij} are lifetime of level 2 and the dipole element between level i and level j at the concentration 3%). For these two models, two cases in the absence or present of a coupling field were considered.

At first, we calculated the absorption and dispersion for the ladder model from Eqs. (7a) and (7b) as a function of Δ_p in the absence of the coupling field E_c with different concentration of Er^{3+} ions as shown in Fig. 2. It can be seen that the absorption and the dispersion for 15 at% Er^{3+} ions is greater than those obtained under other concentrations. In the case of the presence of the coupling field and $\Delta_c = 0$, the calculation results are shown in Fig. 3, which shows that, near the region $\Delta_p = 0$, the absorption and dispersion changed dramatically with Er^{3+} concentration. The absorption for 3 and 0.5 at% Er^{3+} ions approaches to zero. We can see that EIT disappears for 100 at% Er^{3+}:YAG under the intensity of the coupling field, which is due to the coupling field not being strong enough to separate the two peaks of the Autler–Townes splitter. According to the results of numerical calculation in Figs. 2 and 3, when $\Delta_p = 0$, we obtained the ratios of absorption with the coupling field to that without the coupling field. The ratios for 0.5, 3, 15, 33 and 100 at% Er^{3+}:YAG are 0.047%, 0.038%, 0.74%, 7.96% and 87.1%, respectively. This indicates that the relative transmission ratio reaches the maximum at Er^{3+}

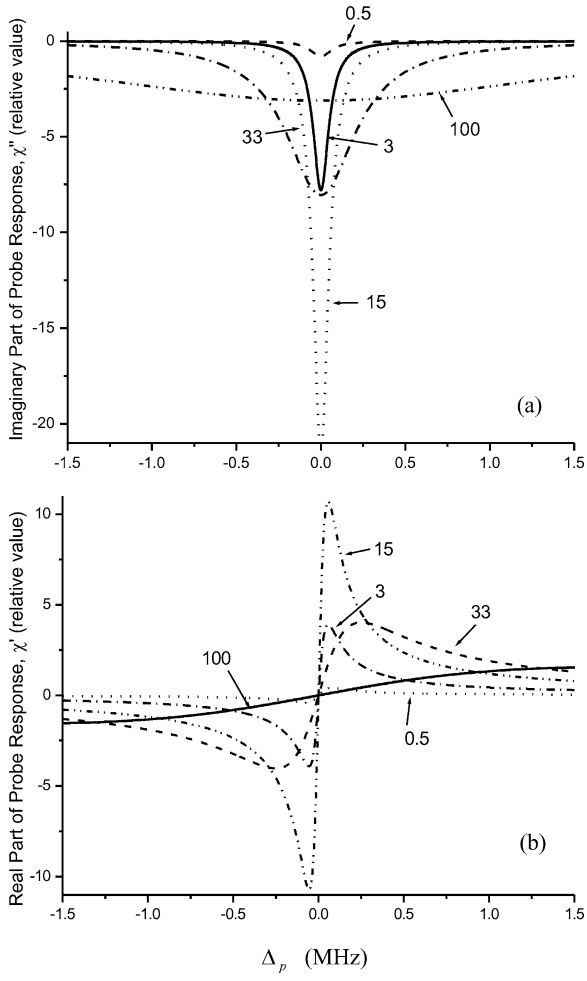

Fig. 2. (a) Imaginary and (b) real part of probe response versus detuning Δ_p in the ladder model in the absence of the coupling field. The numbers represent the concentration of doped Er^{3+} ion.

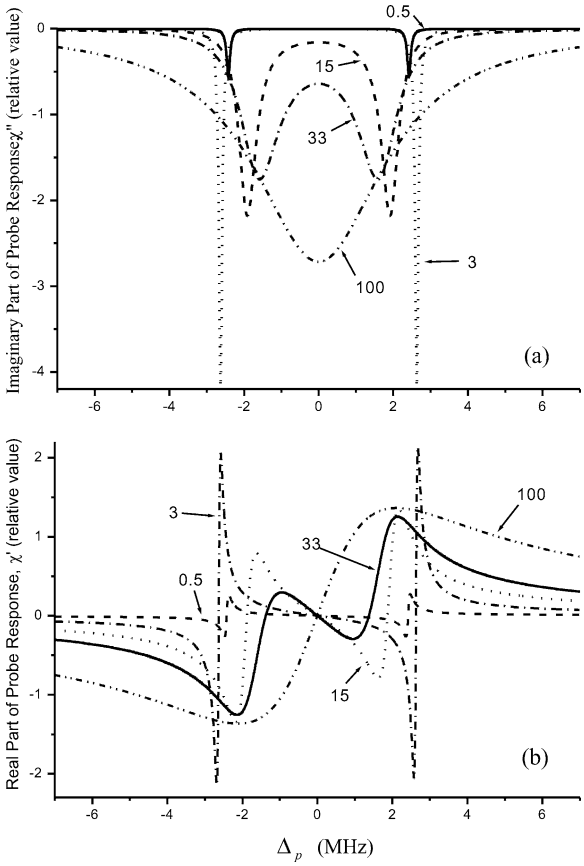

Fig. 3. (a) Imaginary and (b) real part of probe response versus detuning Δ_p in the presence of the coupling field ($\Delta_c = 0$) for the ladder model.

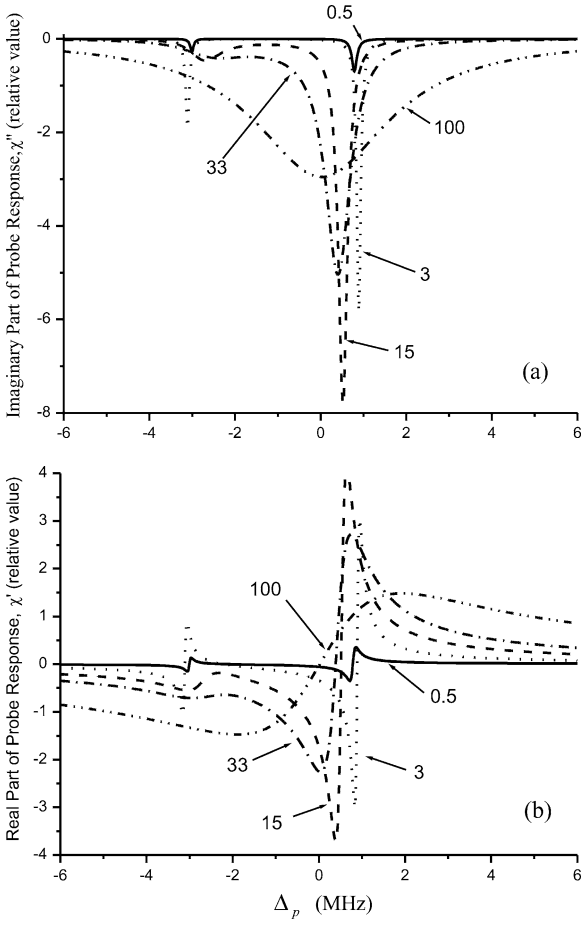

Fig. 4. (a) Imaginary and (b) real part of probe response versus detuning Δ_p in the presence of the coupling field ($\Delta_c \neq 0$) for the ladder model.

concentration of about 3%. Fig. 4 shows the effect of concentration on EIT in the detuning of coupling field ($\Delta_c = 20/\tau_2$, where τ_2 is the lifetime of the level $|2\rangle$ with 3 at% Er:YAG). We can see, from Fig. 4, that the concentration at about 15% near the region $\Delta_p = 0$ is better than others when one wants a large dispersion with relatively small absorption.

For the Λ model, the calculation is analogous to that of the ladder model except for the parameter G_p. Figs. 5 and 6 show the numerical calculation results of the Λ model for $\Delta_c = 0$ and $\Delta_c \neq 0$, respectively. The better concentration value for EIT is similar to that obtained from the ladder model. In contrast to the result in Fig. 3, the inset in Fig. 5 shows two separated peaks of the Autler–Townes splitter for 100 at% Er^{3+}:YAG under the same intensity of the coupling field applied as the case in Fig. 3. This indicates that it is easier to induce EIT in this model than the ladder model. From both models, it shows clearly that the profile of the absorption and the refractive index is greatly changed with the increment of the Er^{3+} concentration.

4. Summary

In this Letter, we have analyzed the concentration effect of Er^{3+} ions on EIT in Er^{3+}:YAG using density matrix equations of interaction between ion and field. We found that the concentration can dramatically affect the depth of EIT window and there exists an optimal concentration to realize the EIT in Er^{3+}:YAG. It

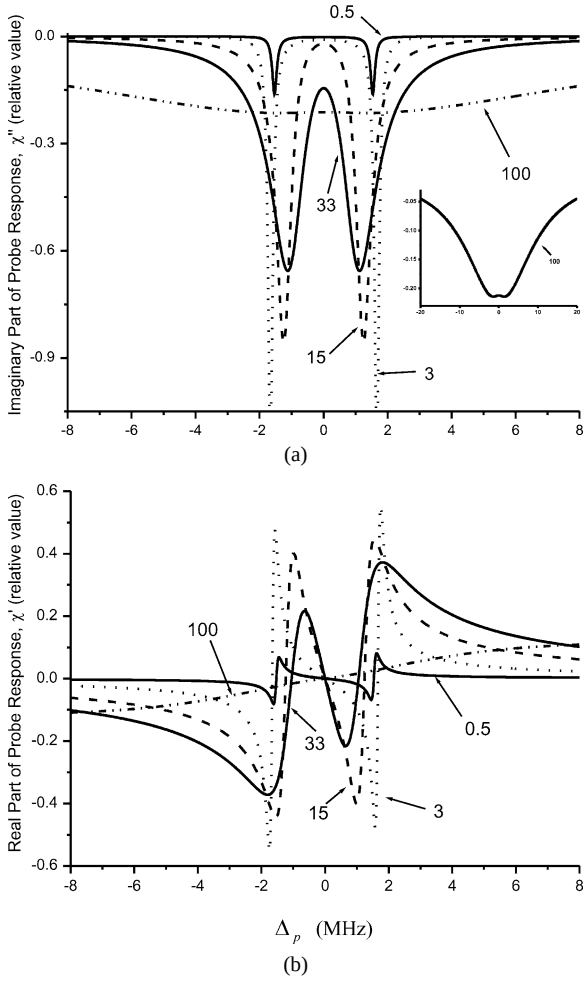

Fig. 5. (a) Imaginary and (b) real part of probe response versus detuning Δ_p for the model with the coupling field ($\Delta_c = 0$). The inset shows the same data for 100 at% Er^{3+}:YAG with another scale.

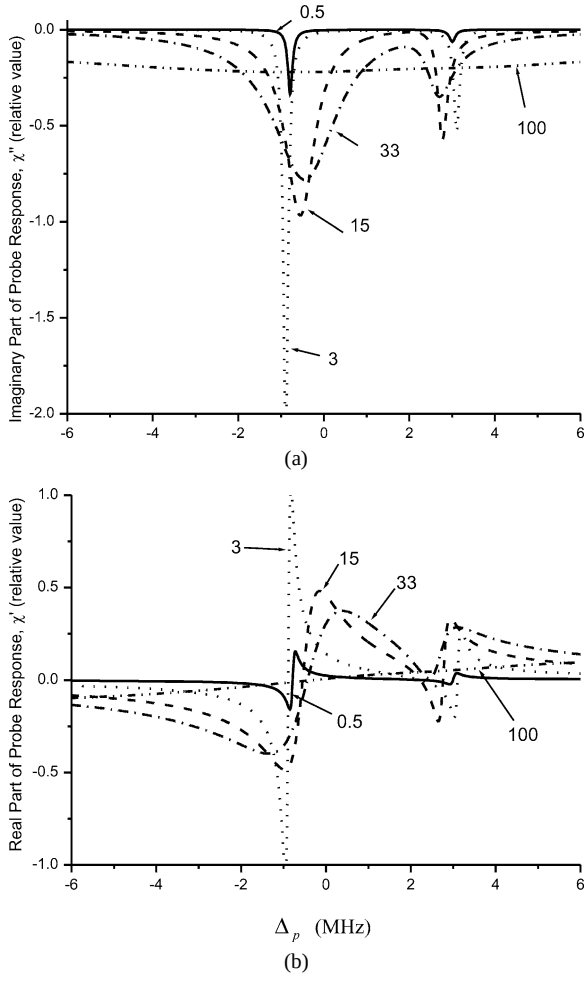

Fig. 6. (a) Imaginary and (b) real part of probe response versus detuning Δ_p for the Λ model with the coupling field ($\Delta_c \neq 0$).

is also demonstrated that there is a region of concentration at which the crystal has a higher dispersion and lower absorption when $\Delta_c \neq 0$. Comparing the results of the two models, we found that the Λ model is easier to induce EIT than the ladder model. These results are helpful to perform EIT in many applications, for example, high-density optical memory, high gain phase conjugation and quantum switching [13–15].

The YAG crystal is an excellent optical host material compared with other compounds, which are sensitive to moisture. Therefore, it is interesting to investigate EIT in this kind of compound for practice applications. In the present Letter, we have reported a preliminary study of EIT in Er^{3+}:YAG and provide a basis for choosing the concentration to carry out experimental studies in the future.

Acknowledgements

The authors are grateful to the financial support from the National Natural Science Foundation of China (No. 10074020) and the Young Teacher Foundation of Jilin University.

References

[1] K.J. Boller, A. Imamoglu, S.E. Harris, Phys. Rev. Lett. 66 (1991) 2593.
[2] M. Xiao, Y.Q. Li, S.Z. Jin, J. Gea-Banacloche, Phys. Rev. Lett. 74 (1995) 666.
[3] S. Shepherd, D.J. Fulton, M.H. Dunn, Phys. Rev. A 54 (1996) 5394.
[4] J.R. Boon, E. Zekou, D.J. Fulton, M.H. Dunn, Phys. Rev. A. 57 (1998) 1323.
[5] A. Imamoglu, S.E. Harris, Opt. Lett. 14 (1989) 1344.
[6] A.S. Zibrov, M.D. Lukin, D.E. Nikonov, L. Hollberg, M.O. Scully, V.L. Velichansky, H.G. Robinson, Phys. Rev. Lett. 75 (1995) 1499.
[7] M.O. Scully, Phys. Rev. Lett. 67 (1991) 1855.
[8] L.V. Hau, S.E. Harris, Z. Dutton, C.H. Behroozi, Nature (London) 397 (1999) 594.
[9] Y. Zhao, C. Wu, B.S. Ham, M.K. Kim, E. Awad, Phys. Rev. Lett. 79 (1997) 641.
[10] B.S. Ham, M.S. Shahriar, P.R. Hemmer, Opt. Lett. 22 (1997) 1138.
[11] B.S. Ham, P.R. Hemmer, M.S. Shahriar, Opt. Commun. 144 (1997) 227.
[12] K. Ichimura, K. Yamamoto, N. Gemma, Phys. Rev. A 58 (1998) 4116.
[13] B.S. Ham, M.S. Shahriar, M.K. Kim, P.R. Hemmer, Opt. Lett. 22 (1997) 1849.
[14] B.S. Ham, P.R. Hemmer, M.S. Shahriar, Phys. Rev. A 59 (1999) R2583.
[15] B.S. Ham, P.R. Hemmer, Phys. Rev. Lett. 84 (2000) 4080.
[16] J.B. Gruber, M.E. Hills, R.M. Macfarlane, C.A. Morrison, G.A. Turner, Chem. Phys. 134 (1989) 241.
[17] V.I. Zhekov, T.M. Murina, A.M. Prokhorov, M.I. Studenikin, S. Georgescu, V. Lupei, I. Ursu, Sov. J. Quantum Electron. 16 (2) (1986) 274.
[18] B.R. Judd, Phys. Rev. 127 (1962) 750.
[19] G.S. Ofelt, J. Chem. Phys. 37 (1962) 511.
[20] A.A. Kaminskii, V.S. Mironov, A. Kornienko, S.N. Bagaev, G. Boulon, A. Brenier, B.D. Bartolo, Phys. Stat. Sol. A 151 (1995) 231.
[21] Q.Y. Wang, S.Y. Zhang, Y.Q. Jia, J. Alloys Compounds 202 (1993) 1.
[22] H.Y. Ling, Y.Q. Li, M. Xiao, Phys. Rev. A 57 (1998) 1338.